Atomic orientation driven by broadly-frequency-modulated radiation: Theory and experiment

G. Bevilacqua and V. Biancalana
DIISM, Università di Siena, via Roma 56, 53100 Siena, Italy

Y. Dancheva
DSFTA, Università di Siena, via Roma 56, 53100 Siena, Italy

(Received 21 March 2016; published 5 July 2016)

We investigate magnetic resonances driven in thermal vapor of alkali-metal atoms by laser radiation broadly modulated at a frequency resonant with the Zeeman splitting. A model accounting for both hyperfine and Zeeman pumping is developed, and its results are compared with experimental measurements performed at relatively weak pump irradiance. The interplay between the two pumping processes generates intriguing interaction conditions, often overlooked by simplified models.

DOI: 10.1103/PhysRevA.94.012501

I. INTRODUCTION

Optical pumping processes in atomic samples [1] have been the subject of intensive theoretical and experimental studies since the 1960s [2] and have been used in several applications, including laser cooling [3], molecular spectroscopy [4], and atomic magnetometry. Atomic magnetometers are nowadays available as commercial devices, but further research is presently being carried out to optimize the performance, as well as to better understand phenomena and mechanisms which subtly act in this kind of apparatus.

The interest in precise and sensitive magnetic field measurements led to a revival of the research in magnetometry, particularly in the optical-atomic sensors. Optical magnetometers were recently subject to impressive advances in terms of sensitivity. The possibility of absolute field measurements, the low operation costs and power consumption, the robustness, and the potential for miniaturization let these devices compete with superconducting quantum interference devices, traditionally regarded as state-of-the-art magnetometric sensors.

The typical working principle of an atomic optical magnetometer [5] is based on the preparation of an atomic state using optical pumping and on the detection of its time evolution driven by the magnetic field under measurement. Some recent works on atomic magnetometry have addressed time-domain operation techniques, where the atomic state is first prepared and then is followed in its free evolution within the decay time [6]. In contrast, most of the approaches reported in the literature are based on a frequency-domain detection [7]. In this case, a steady-state condition is reached by means of a periodic regeneration of the atomic state to be analyzed. This regeneration is obtained by applying an appropriate optical radiation with some parameter periodically modulated in resonance (or near resonance) with the evolution of the atomic state. Experiments have been reported where the modulated parameter of the pump radiation is its amplitude [8–10], its polarization [11–14], or its optical frequency [15,16]. Different macroscopic quantities have been chosen to be measured as well, such as the absorption [12], the polarization rotation [17–19], or (in similar experiments based on solid-state samples) the fluorescence [20], all opening an indirect way to follow the vapor magnetization.

Optical pumping is often applied in the regime of strong intensity where power broadening and nonlinear dependence on the laser intensity occur. Studies in the low-intensity regime have also been reported [21].

Our study concerns a setup developed for precise atomic magnetometry, which here is operated in a condition of weak excitation intensity. The atomic sample is illuminated by two collinear laser beams. One of them (modulated beam, MB in the following) is frequency modulated and circularly polarized, and the second one (detection beam, DB) is linearly polarized with the polarization plane rotated by the time-dependent circular birefringence of the sample. In other terms, the MB induces a magnetic dipole that precesses at the Larmor frequency, and the dipole component parallel to the beams is monitored.

The MB is broadly modulated in frequency; thus both the ground hyperfine states of the atomic vapor are excited with nonvanishing rates. As far as we know, the application of this method has never been investigated by other researchers. Such broad modulation gives rise to an important interplay between hyperfine and Zeeman pumping that has advantages in optical magnetometry [22]. The proposed excitation scheme not only simplifies the setup (the pump-repump scheme is often applied as an alternative) but has the potential to significantly increase the signal without increasing the magnetic-resonance width, particularly at higher intensities, with obvious practical implications.

In this work we address mainly the aspects related to the wide MB frequency modulation, restricting the investigation to a regime of relatively weak intensity, deferring the analysis of the intense pumping to another study. We develop a model considering the MB interaction with the whole level structure of the D_1 Cs transitions: a point which is often overlooked in the literature. We obtain a modified version of the Larmor equation for the magnetization created in a given ground-state Zeeman multiplet. An analytical expression for the magnetization amplitude, pointing out the dependence on the MB modulation parameters, is found, and it matches very well with the experiment.

This paper is organized as follows: in Sec. II we briefly describe the experimental apparatus; in Sec. III the theoretical

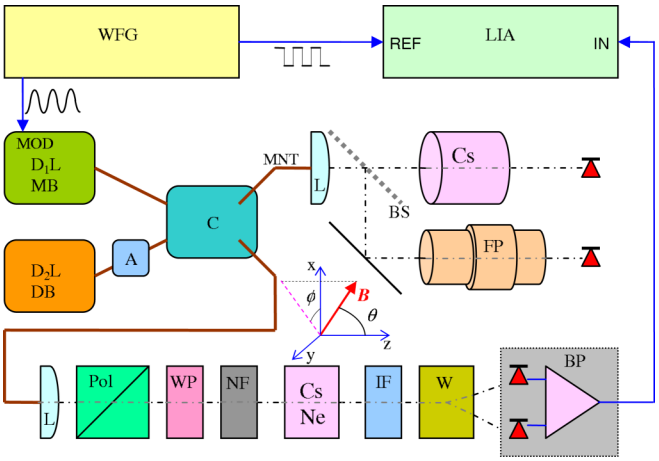

FIG. 1. Schematics of the setup. WFG, waveform generator; D_1L, pumping laser (MB) at 894 nm; D_2L (DB), detection laser at 852 nm; A, attenuator; C, single mode, polarization maintaining 2×2 fiber coupler; L, lens, BS, beam splitter, Pol, polarizer; WP, multiorder wave plate acting as quarter-λ plate for 894 nm and as a full-λ plate for 852 nm; NF, neutral filter; Cs-Ne, cesium cell with buffer gas; IF, interference filter stopping 894 nm; W, Wollaston analyzer; BP, balanced polarimeter for polarization rotation detection, which includes photo diodes and a differential transimpedance amplifier; LIA, lock-in amplifier. In the monitor (MNT) channel, Cs (the cesium vacuum cell) and FP (the Fabry-Pérot interferometer) are used to monitor the radiation parameters.

model is reported. Finally, in Sec. IV we discuss and compare the theoretical and the experimental results.

II. EXPERIMENTAL SETUP

A detailed description of the experimental setup is given in Refs. [18,22]. Briefly, Cs vapor is contained in a sealed cell, where buffer gas is added to counteract time-of-flight line broadening of the magnetic resonances and to increase the optical pumping effect. The Cs atoms are optically pumped by a circularly polarized, near-resonant laser (MB) light at 894 nm (D_1 Cs line). The cell is at room temperature and in a highly homogeneous magnetic field. A balanced polarimeter enables the detection of the atomic precession, which causes the polarization rotation of a linearly polarized beam (DB), nearly resonant with the $F_g = 4$ to $F_e = 3, 4, 5$ group of transitions belonging to the Cs D_2 line. The setup contains two channels (see Fig. 1), which in magnetometric applications [23–25] are used to reject common-mode magnetic noise and to measure local magnetic variations by means of a differential method. In the present work one of the channels is used to detect the atomic spin precession, while the other one (monitor, MNT) is used for precise determination of the DB and MB intensities and absolute frequencies. The DB radiation is attenuated down to 10 nW and kept at a constant frequency, blue detuned by about 2 GHz with respect to the D_2 transition set starting from $F_g = 4$. The MB radiation, which in magnetometric applications was in the milliwatt range, here is attenuated down to 100 nW, and its optical frequency is made time dependent through a junction current modulation at a frequency matching (or ranging around) the Larmor frequency. Both the MB and DB have a circular beam spot about 1cm^2 in size.

The optical frequency of the MB is monitored by the MNT channel, where the light is sent to a fixed-length Fabry-Pérot interferometer and to a secondary Cs cell without buffer gas. Both the absorption and the interferometric signals are detected by photodetection stages with a bandpass largely exceeding the MB modulation frequency. The two diagnostics provide both a relative and an absolute measure of the instantaneous detuning of the MB frequency. The (fixed) DB optical frequency is monitored as well, and it is passively stabilized within 100 MHz.

A sinusoidal signal modulates the optical frequency of the MB at the Larmor frequency and references a lock-in amplifier detecting the polarization rotation of the DB. The Cs cell is placed in a bias magnetic field of about 600 nT resulting from the partial compensation of the environmental field. Such bias field results in a Cs magnetic resonance centered at about 2 kHz. The amplitude of the magnetic resonance is registered for various amplitudes of the modulation signal and as a function of the mean MB optical frequency. To this aim the MB optical frequency is slowly scanned by adding a ramp to its modulation signal.

III. MODEL

To develop a theoretical model that describes the time evolution of the monitored magnetization, we consider the whole level structure of the ^{133}Cs D_1 line. With reference to Fig. 2, the free Hamiltonian in the rotating-wave approximation frame

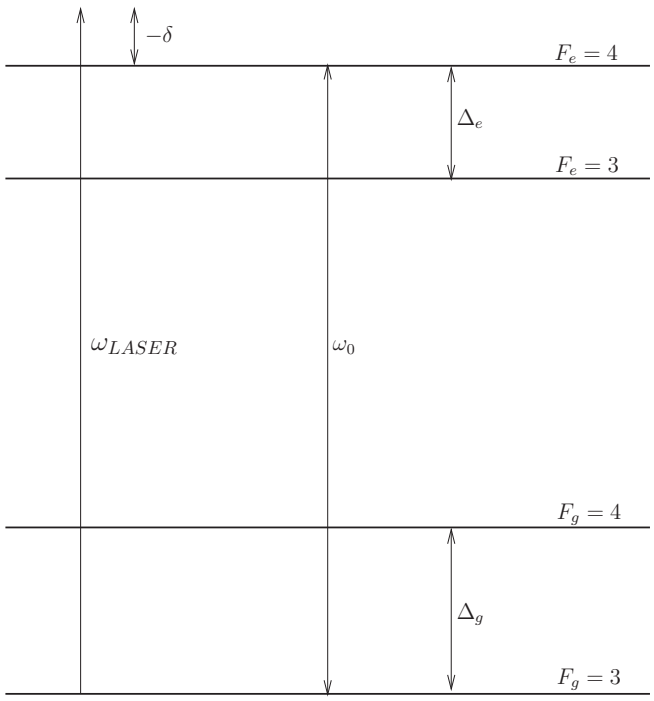

FIG. 2. Simplified level scheme of the Cs D_1 line. The frequency of the $F_g = 3 \rightarrow F_e = 4$ transition is labeled ω_0. The instantaneous detuning $\delta(t)$ of the MB is outlined. Notice that δ is varied by a large amount so that the MB radiation can become resonant with each transition. The DB radiation monitors the $F_g = 4$ magnetization; it is resonant with the D_2 line and is not shown.

reads

$$H_0 = \Delta_g\, \Pi_{g4} + \delta\, \Pi_{e4} + (\delta - \Delta_e)\, \Pi_{e3}, \tag{1}$$

where the projector Π_{g4} is defined as $\sum_M |F_g = 4, M\rangle\langle F_g = 4, M|$. Similar expressions hold for the other projectors.

To express the interaction with the laser field it is better to adopt a block-matrix notation,

$$H_{\rm int} = \begin{pmatrix} 0 & 0 & W^\dagger_{e4,g4} & W^\dagger_{e4,g3} \\ 0 & 0 & W^\dagger_{e3,g4} & W^\dagger_{e3,g3} \\ W_{g4,e4} & W_{g4,e3} & 0 & 0 \\ W_{g3,e4} & W_{g3,e3} & 0 & 0 \end{pmatrix}, \tag{2}$$

where each matrix element is a submatrix defined using the projectors. For instance, $W^\dagger_{e4,g4} = -\Pi_{e4}\, \mathbf{d}\cdot\boldsymbol{\epsilon}\, \Pi_{g4}\, E_0$, $W_{g4,e4} = -\Pi_{g4}\, \mathbf{d}\cdot\boldsymbol{\epsilon}^*\, \Pi_{e4}\, E_0$, etc. Here $\boldsymbol{\epsilon}$ is the laser polarization versor, E_0 is the amplitude of the laser electric field, and $\mathbf{d}$ is the atomic dipole moment.

We need all these blocks in our model because the laser modulation can be very broad and during the periodic frequency sweep both the ground states may be resonantly excited.

The density operator has a similar block-matrix form,

$$\boldsymbol{\rho} = \begin{pmatrix} \rho_{e4} & \rho_{e4,e3} & \rho_{e4,g4} & \rho_{e4,g3} \\ \rho_{e3,e4} & \rho_{e3} & \rho_{e3,g4} & \rho_{e3,g3} \\ \rho_{g4,e4} & \rho_{g4,e3} & \rho_{g4} & \rho_{g4,g3} \\ \rho_{g3,e4} & \rho_{g3,e3} & \rho_{g3,g4} & \rho_{g3} \end{pmatrix}. \tag{3}$$

The blocks are defined in the manner described above. The diagonal blocks $\rho_{e4}, \rho_{e3}, \rho_{g4}$, and ρ_{g3} contain both the level populations and the Zeeman coherences. The blocks $\rho_{e4,e3} = \rho^\dagger_{e3,e4}$ and $\rho_{g4,g3} = \rho^\dagger_{g3,g4}$ represent the hyperfine coherences, while the remaining blocks represent the optical coherences.

We assume that the hyperfine coherences can be neglected (secular approximation), and with standard methods we write the Bloch equation:

$$\dot{\boldsymbol{\rho}} = -i[H_0 + H_{\rm int}, \boldsymbol{\rho}] + \mathcal{L}_D\, \boldsymbol{\rho}, \tag{4}$$

where the Liouvillian $\mathcal{L}_D$ takes into account the effects of relaxation processes like spontaneous emission and/or collisions.

As the magnetization is monitored by the DB tuned in the vicinity of the $F_g = 4 \rightarrow J_e = 3/2$ transition, the signal is substantially given by the $|F_g = 4\rangle$ state. We assume that the effect of the DB is very weak and its contribution to the Hamiltonian can be neglected. Hence the Bloch equation (4) contains only the MB interaction. To some extent, this approximation is relaxed in the following (see the Appendix).

After some algebra and introducing the irreducible components [2,26]

$$\rho_{g4} = \sum_{k=0}^{2F_{g4}} \sum_{q=-k}^{k} m_{k,q}\; T_{k,q}(g4) \tag{5}$$

in the hypothesis of the weak-laser-power regime, we find the final equation for the ground-state $F_g = 4$ orientation:

$$\dot{\mathbf{x}} = i\frac{\omega_L}{\sqrt{2}} \begin{pmatrix} -\sqrt{2}(\cos\theta + \gamma) & \sin\theta e^{i\phi} & 0 \\ \sin\theta e^{-i\phi} & -\sqrt{2}\gamma & \sin\theta e^{i\phi} \\ 0 & \sin\theta e^{-i\phi} & \sqrt{2}(\cos\theta - \gamma) \end{pmatrix} \mathbf{x} + P(t) \begin{pmatrix} 0 \\ 1 \\ 0 \end{pmatrix} = A\,\mathbf{x} + P(t)\mathbf{w}, \tag{6}$$

where the vector $\mathbf{x}$ is defined as $\mathbf{x} = (m_{1,-1}, m_{1,0}, m_{1,1})$.

The model produces equations for both the magnetization (orientation) and the alignment; however, in this work we discuss only the dynamics of the orientation.

The pumping rate $P(t)$ is reported in the Appendix with full derivation details. Notice that Eq. (6) is essentially equivalent to the Larmor equation with an additional forcing term, because $M_x \propto (m_{1,1} - m_{1,-1})$, $M_y \propto i(m_{1,1} + m_{1,-1})$, and $M_z \propto m_{1,0}$.

The Larmor frequency is $\omega_L = g_{Fg}\mu_B B$. In our experiment ω_L is in the kilohertz range, while the relaxation rates (longitudinal and transverse) are in hertz range, so in Eq. (6) we used a single rate γ. The geometry considered in the model is sketched in Fig. 1.

The matrix of coefficients in Eq. (6) can be diagonalized by a Wigner rotation [27] matrix U so that

$$U^\dagger\, A\, U = A_D = \begin{pmatrix} -i\omega_L - \gamma & 0 & 0 \\ 0 & -\gamma & 0 \\ 0 & 0 & i\omega_L - \gamma \end{pmatrix}, \tag{7}$$

and the full solution is

$$\mathbf{x}(t) = U e^{A_D t} U^\dagger\, \mathbf{x}(0) + U \int_0^t e^{A_D(t-t')} P(t')dt'\; U^\dagger \mathbf{w}. \tag{8}$$

After a time interval much longer than $1/\gamma$, the free solution fades away, and the steady-state orientation $\mathbf{x}_{ss}$ is determined by the last term. Introducing the Fourier components of the pumping term

$$P(t) = \sum_{n=-\infty}^{+\infty} P_n e^{i\,n\,\Omega\,t}, \tag{9}$$

where $\Omega \approx \omega_L$ is the modulation frequency, one has

$$\mathbf{x}_{SS} = \sum_{n=-\infty}^{+\infty} P_n \left(U\, \frac{1}{i\,n\,\Omega - A_D}\, U^\dagger \right) \mathbf{w}\, e^{i\,n\,\Omega t}. \tag{10}$$

We are interested in the z component of the magnetization, so after some straightforward algebra we find

$$\begin{aligned} M_z^{SS}(t) \propto\; & \mathrm{Re}(P_0 C_0) + \sum_{n=1}^{+\infty} [\mathrm{Re}(P_n C_n + P_{-n} C_{-n})\, \cos n\Omega t \\ & - \mathrm{Im}(P_n C_n - P_{-n} C_{-n})\, \sin n\Omega t] \\ \equiv\; & a_0 + \sum_n [a_n \cos n\Omega t + b_n \sin n\Omega t], \end{aligned} \tag{11}$$

where

$$C_n = \frac{\sin^2\theta}{2}\left(\frac{1}{i\,n\,\Omega+\gamma+i\omega_L}+\frac{1}{i\,n\,\Omega+\gamma-i\omega_L}\right) + \frac{\cos^2\theta}{i\,n\,\Omega+\gamma}. \tag{12}$$

In the experiment, the lock-in amplifier detects the amplitude of the first harmonic ($n=1$), so we have to evaluate the term $\sqrt{a_1^2+b_1^2}$. The coefficients P_n satisfy $P_{-n}=P_n^*$ for each n. Additionally, for odd values of n we have $P_{-n}=P_n^*=-P_n$, meaning that for $n=1$ we can assume $P_1=iR_1$ and $P_{-1}=-iR_1$ (R_1 is a real quantity reported in the Appendix).

Using the condition $\Omega\approx\omega_L$ and $\theta=\pi/2$, $\phi=0$ (given by the experimental conditions), after some algebra one finds

$$\mathcal{A}_1 \equiv \sqrt{a_1^2+b_1^2} = \frac{1}{\gamma^2+(\Omega-\omega_L)^2}\,|R_1|. \tag{13}$$

Equation (13) has a clear physical meaning: at low laser power the response of the system is factored out. The first factor gives the usual resonant behavior when the modulation frequency Ω is swept over the magnetic resonance line. The second term R_1 contains the details of the laser frequency modulation and the level structure of the D_1 lines.

The optical frequency of the MB is sinusoidally modulated at the magnetic resonance frequency, so that $\Omega\simeq\omega_L$ and the laser detuning δ from the D_1 $F_g=3\longrightarrow F_e=4$ transition (see also Fig. 2) is

$$\delta(t)=\delta_0+\Delta\sin\omega_L t. \tag{14}$$

It follows that R_1 is a function of both δ_0 and Δ. Moreover it depends also on the width of the D_1 one-photon transition $G=\Gamma/2+\Gamma_c+\Gamma_D$, where $1/\Gamma$ is the radiative lifetime of the excited D_1 multiplet, Γ_c represents the broadening due to collisions, and Γ_D is the Doppler broadening. Due to the presence of buffer gas, the excited D_1 states get depolarized with an additional rate Γ_c', which we added as a phenomenological dependence in R_1 in a normalized form, $r=\Gamma_c'/\Gamma$. Finally, to model the influence of the DB, a parameter α, describing a global population imbalance of the two ground hyperfine states, is also introduced.

The Appendix contains a full derivation and discussion of the explicit form of R_1, as well as a detailed definition of the parameter α.

IV. RESULTS

In this section we report experimental measurements obtained in different regimes and compare them with the theoretical profiles.

Besides atomic constants, the model contains several parameters (δ_0, Δ, r, and G) fixed by the experimental conditions and only one quantity, α, which is a free parameter. In our conditions $\Gamma\approx 5$ MHz, and the broadening due to collisions is dominant, as $\Gamma_c\approx 500$ MHz at 90 Torr of He and $\Gamma_D\approx 200$ MHz; thus we use $G=0.5$ GHz in almost all the simulations.

Concerning r, it has been known since the 1960s [28,29] that the collisions with the buffer-gas atoms are effective in depolarizing the D_2 excited states, while perturbing weakly the $D_1^2P_{1/2}$ states. Moreover, our theoretical results do not depend strongly on the value of r, and we have assumed $r=0.5$ in all the simulations.

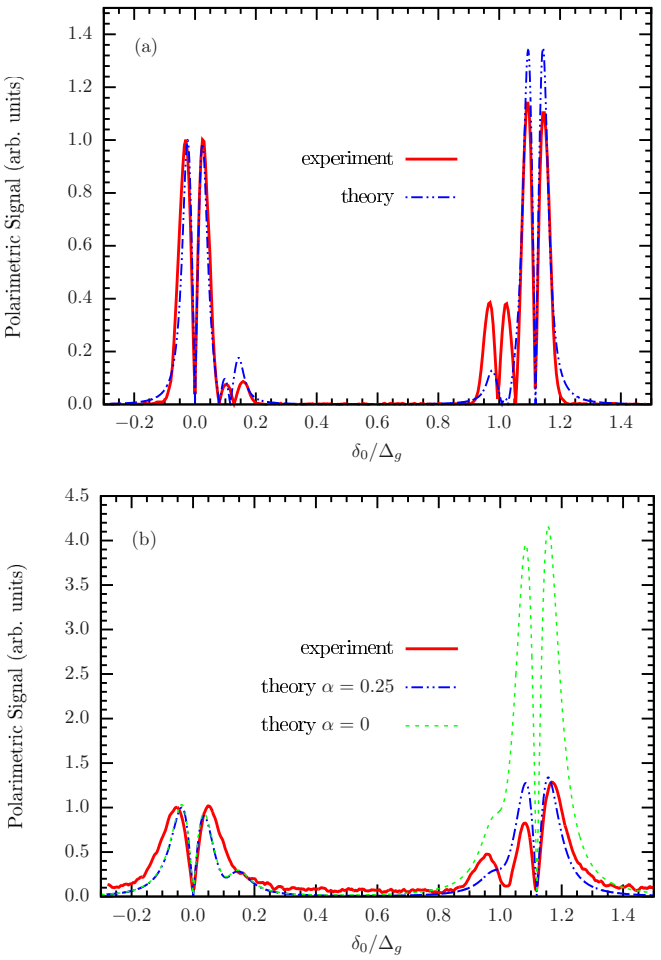

FIG. 3. Comparison of theoretical and experimental signals as a function of δ_0/Δ_g in a regime of small modulation. For both plots the following values have been used in the model: $2\Delta=0.5$ GHz, $r=0.5$, $\alpha=0.25$, $\Delta_e=1.1$ GHz, and $\Delta_g=9.2$ GHz. The plots show magnetic resonance amplitudes as obtained with (a) low buffer-gas pressure (2 Torr Ar) and (b) high buffer-gas pressure (90 Torr Ne). Correspondingly, $G=200$ MHz and $G=500$ MHz are used in the simulations. In (b) we also report for comparison the model output obtained with $\alpha=0$.

The only free parameter, α, is chosen to obtain the best correspondence between the measured and simulated signals. As shown below, a value of $\alpha\approx 0.25$ leads to a good comparison, a clear indication that, in spite of its very low power, DB has a not negligible influence.

As for the modulation amplitude Δ, it has to be compared to Δ_g, and three regimes can be identified: small ($2\Delta\ll\Delta_g$), intermediate ($2\Delta\approx\Delta_g$), and large ($2\Delta\gg\Delta_g$) modulation amplitudes. In the following we discuss these three regimes.

Figure 3 shows the signal obtained for $\Delta=0.5$ GHz. As predicted by Eq. (A15), the four D_1 transitions give eight peaks in R_1, separated into two groups around the positions of the two hyperfine ground states, corresponding to $\delta_0/\Delta_g\approx 0$ and $\delta_0/\Delta_g\approx 1$. These peaks are well resolved in conditions

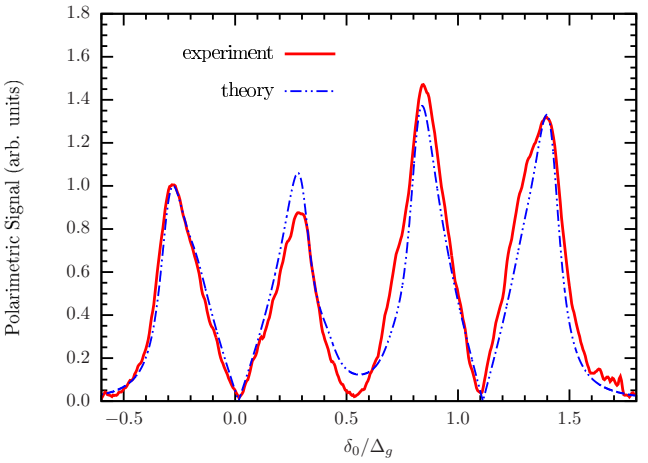

FIG. 4. Comparison of theoretical and experimental signals as a function of δ_0 in the intermediate regime. The following values have been used: $G = 0.5$ GHz, $2\Delta = 5.6$ GHz, $\Gamma_c'/\Gamma = 0.5$, $\alpha = 0.25$, $\Delta_e = 1.1$ GHz, and $\Delta_g = 9.2$ GHz.

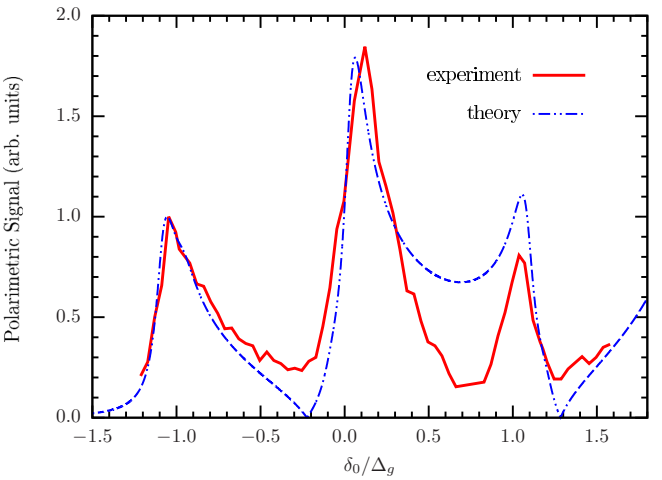

FIG. 5. Comparison between theoretical and experimental signals as a function of δ_0 in the regime with $2\Delta \gg \Delta_g$. The following values have been used: $G = 0.5$ GHz, $2\Delta = 20.0$ GHz, $\Gamma_c'/\Gamma = 0.5$, $\alpha = 0.20$, $\Delta_e = 1.1$ GHz, and $\Delta_g = 9.2$ GHz.

of small collisional broadening, as can be seen in Fig. 3(a). Here the experimental signal is recorded with a lower buffer-gas pressure giving a nominal $\Gamma_c \approx 18$ MHz, so to compare we used the value $G = 200$ MHz. Increasing the collisional broadening up to 0.5 GHz, some peaks overlap, as can be seen in Fig. 3(b).

In all the plots, we normalize to 1 the height of the leftmost peaks, both measured and simulated. The value of α is chosen in such a way to reproduce the rightmost peak's height matching the experimental observation. With $\alpha = 0$ the right peak is four times higher than the first one [see the green dashed line in Fig. 3(b)]. Good agreement between the measured and simulated resonance amplitudes is found for $\alpha \approx 0.25$.

It is remarkable that when the MB is mainly resonant with the $F_g = 3$ transitions (e.g., $\delta_0 \approx -\Delta$), the recorded signal has a peak value comparable with the one obtained with $\delta_0 \approx \Delta_g$, in spite of the fact that the measured quantity is the magnetization in the $F_g = 4$ ground state. At $\delta_0 \approx -\Delta$, the MB causes a strong hyperfine pumping towards the $F_g = 4$ state. Thus, despite the fact that the laser is not in resonance with the $F_g = 4$ sublevels, a high degree of Zeeman pumping is observed. Thus the leftmost peak appearing in the plot corresponds to an interaction condition where the MB produces a high-amplitude magnetic resonance while weakly perturbing the hyperfine ground state where the magnetization is induced. This interaction regime has been successfully used (in a regime of stronger MB intensity) for high-sensitivity magnetometry [22].

As shown in Fig. 4, the model reproduces with good accurateness the signal behavior also in the intermediate regime where $2\Delta \approx \Delta_g$. In this case, the MB may resonantly excite either one or both of the ground states simultaneously, which happens for $\delta_0/\Delta_g \approx 1/2$. Good agreement between the theoretical and experimental results is obtained while keeping the same values of the parameters. In this case the eight components merge into four peaks of comparable height and nearly symmetric shape.

The results corresponding to the third regime, where 2Δ exceeds Δ_g, are shown in Fig. 5. Here some technical limitations prevent the possibility to extend the scan at higher values of δ_0, so that the rightmost peak corresponding to L_{eg} [see Eq. (A3d)] is not recorded. The leftmost peak has a maximum at $\delta_0 \approx -\Delta$, according to what is expected from Eq. (A3). The peaks observed experimentally have an asymmetric shape more evident at large values of Δ; this feature is well reproduced by the model. On the other hand, similar to what appears in Fig. 3, some discrepancies emerge more visibly at $\delta_0 \approx \Delta_g$. There is experimental evidence that the DB, in spite of its very weak intensity, is responsible for these minor deviations: those discrepancies actually depend on the intensity and on the detuning of DB, becoming more evident under conditions of stronger interaction.

V. CONCLUSION

A model is developed to describe the behavior of magnetic resonances measured in cesium vapor in an experiment where a weak-intensity laser radiation tuned to the D_1 transitions is broadly frequency modulated. Such modulation makes the laser-atom interaction occur in a condition where both the hyperfine ground levels are excited. In the approximation of weak intensity, a multipole expansion analysis enables an accurate evaluation of the measured quantity that is the time-dependent magnetization of atoms in the $F_g = 4$ state. A comparison with the experiment is made in three regimes, where the modulation depth is smaller than, comparable to, or larger than the ground-state hyperfine splitting. Good correspondence is found, and the model reproduces satisfactorily the recorded features with the requirement of tuning only one free parameter (α). This parameter is phenomenologically introduced to account for an imbalance in the populations of the $F_g = 3$ and $F_g = 4$ states that is induced by the detection radiation.

APPENDIX: DERIVATION OF THE PUMPING TERM

Rewriting Eq. (4) for each block of $\boldsymbol{\rho}$ and assuming the adiabatic approximation [30] for the optical coherences, for instance, we find

$$\rho_{e_4,g_4} = \frac{i}{G + i(\delta - \Delta_g)} \left[\rho_{e4,e4}\, W^{\dagger}_{e4,g4} - W^{\dagger}_{e4,g4}\, \rho_{g4,g4}\right] \quad \text{(A1)}$$

and similar expressions for the other optical coherences, which we do not report explicitly. In (A1) G is the width of the D_1 one-photon transition determined as $G = \Gamma/2 + \Gamma_c$ ($1/\Gamma$ is the lifetime of the excited D_1 multiplet, and Γ_c represents additional broadening due to collisions). Finally, δ is the laser detuning from the $F_g = 3 \to F_e = 4$ transition (see also Fig. 2).

Substituting expressions like (A1) in the equations for the diagonal blocks of $\boldsymbol{\rho}$, we find

$$\begin{aligned}\dot{\rho}_{e4} = &-\Gamma\rho_{e4} + \mathcal{L}_{\rm coll}(\rho_{e4}) \\ &- i[D_0 W^{\dagger}_{e4,g3} W_{g3,e4} + D_g W^{\dagger}_{e4,g4} W_{g4,e4}, \rho_{e4}] \\ &- \{L_0 W^{\dagger}_{e4,g3} W_{g3,e4} + L_g W^{\dagger}_{e4,g4} W_{g4,e4}, \rho_{e4}\} \\ &+ 2L_0 W^{\dagger}_{e4,g3}\, \rho_{g3}\, W_{g3,e4} + 2L_g W^{\dagger}_{e4,g4}\, \rho_{g4}\, W_{g4,e4},\end{aligned} \quad \text{(A2a)}$$

where $\mathcal{L}_{\rm coll}$ takes into account the collision effects in the excited state. We assume that $\mathcal{L}_{\rm coll}$ is diagonal and quenches the multipoles with $k \geqslant 1$ (see below).

Similarly, one obtains

$$\begin{aligned}\dot{\rho}_{g4} = &-\gamma\rho_{g4} - i[-\boldsymbol{\mu}\cdot\mathbf{B}, \rho_{g4}] \\ &- i[D_g W_{g4,e4} W^{\dagger}_{e4,g4} + D_{eg} W_{g4,e3} W^{\dagger}_{e3,g4}, \rho_{g4}] \\ &- \{L_g W_{g4,e4} W^{\dagger}_{e4,g4} + L_{eg} W_{g4,e3} W^{\dagger}_{e3,g4}, \rho_{g4}\} \\ &+ 2L_g W_{g4,e4}\, \rho_{e4}\, W^{\dagger}_{e4,g4} \\ &+ 2L_{eg} W_{g4,e3}\, \rho_{e3}\, W^{\dagger}_{e3,g4} + \mathcal{R}_{s.e.}.\end{aligned} \quad \text{(A2b)}$$

Analogous expressions are obtained for the other diagonal blocks of $\boldsymbol{\rho}$. From Eq. (A2) we can infer that the laser gives a Hamiltonian contribution (the term with the commutator) as well as a relaxation (the term with the anticommutator) to the dynamics of the excited- and ground-state multiplets. In (A2) we have introduced the abbreviations

$$\frac{1}{G + i\delta} = L_0 - i D_0, \quad \text{(A3a)}$$

$$\frac{1}{G + i(\delta - \Delta_e)} = L_e - i D_e, \quad \text{(A3b)}$$

$$\frac{1}{G + i(\delta - \Delta_g)} = L_g - i D_g, \quad \text{(A3c)}$$

$$\frac{1}{G + i(\delta - \Delta_g - \Delta_e)} = L_{eg} - i D_{eg}, \quad \text{(A3d)}$$

and $\mathcal{R}_{s.e.}$ represents the spontaneous emission contributions, whose explicit expressions in terms of irreducible components (see below) are reported by Dumont [31]. In addition, we neglect the excited-state dynamics due to the magnetic field and add a phenomenological relaxation constant γ in the ground state.

To proceed further we assume the low-laser-power limit and completely unpolarized ground states

$$W \to \eta W, \quad \text{(A4a)}$$

$$W^{\dagger} \to \eta W^{\dagger}, \quad \text{(A4b)}$$

$$\rho_{e4} = \eta^2 \rho^{(2)}_{e4} + O(\eta^4), \quad \text{(A4c)}$$

$$\rho_{e3} = \eta^2 \rho^{(2)}_{e3} + O(\eta^4), \quad \text{(A4d)}$$

$$\rho_{g4} = \left(\frac{1}{2} - \alpha\right)\frac{\Pi_{g4}}{2F_{g4}+1} + \eta^2 \rho^{(2)}_{g4} + O(\eta^4), \quad \text{(A4e)}$$

$$\rho_{g3} = \left(\frac{1}{2} + \alpha\right)\frac{\Pi_{g3}}{2F_{g3}+1} + \eta^2 \rho^{(2)}_{g3} + O(\eta^4), \quad \text{(A4f)}$$

where η is a very small parameter quantifying the approximation. Here the factors $1/2 \pm \alpha$ ($-1/2 \leqslant \alpha \leqslant 1/2$) account, in a phenomenological way, for the pumping effects of the DB. When $\alpha = 0$, the DB is an ideal probe laser not disturbing the ground-state dynamics. A positive value of α denotes an increase of the $F_g = 3$ global population and a decrease of the $F_g = 4$ one. A negative value of α would denote the opposite. Introducing the population imbalance in such a simplified way corresponds to neglecting the Zeeman sublevel structure of the ground states and the details of their interaction with the DB: in other words, $\alpha \neq 0$ reproduces only a global population imbalance between the two hyperfine ground states while excluding any polarization effect.

To proceed it is better to introduce the irreducible components [2,26] of each density matrix block

$$\rho^{(2)}_{g4} = \sum_{k=0}^{2F_{g4}} \sum_{q=-k}^{k} \left(\rho^{(2)}_{g4}\right)_{k,q} T_{k,q}(g4), \quad \text{(A5)}$$

where the irreducible tensor operators

$$\begin{aligned}T_{k,q}(g4) = \sqrt{2k+1} \sum_{M} (-1)^{F_{g4}-M} \begin{pmatrix} F_{g4} & F_{g4} & k \\ M & q-M & -q \end{pmatrix} \\ \times |F_{g4} M\rangle\langle F_{g4} M - q|\end{aligned} \quad \text{(A6)}$$

are expressed using the Wigner $3j$ coefficients. Similar expressions can be written for the remaining blocks.

The effect of collisional damping in the excited state is modeled as

$$\left[\mathcal{L}_{\rm coll}\left(\rho^{(2)}_{e4}\right)\right]_{k,q} = -\Gamma'_c\, (\rho^{(2)}_{e4})_{k,q} \quad k \geqslant 1. \quad \text{(A7)}$$

The ground-state feeding by spontaneous emission described by $\mathcal{R}_{s.e.}$ in Eq. (A2b) assumes a simple form for the irreducible components [31],

$$[\mathcal{R}_{s.e.}(e \to g)]_{k,q} = \xi_k(J_e, Fe, J_g, Fg)\, (\rho_e)_{k,q}, \quad \text{(A8)}$$

where

$$\xi_k(J_e,F_e,J_g,F_g) = (2J_e+1)(2F_g+1)(2F_e+1)(-1)^{F_e+F_g+k+1}\Gamma \begin{Bmatrix} F_e & F_g & 1 \\ J_g & J_e & I \end{Bmatrix}^2 \begin{Bmatrix} F_g & F_g & k \\ F_e & F_e & 1 \end{Bmatrix}. \tag{A9}$$

After some algebra Eq. (A2b) becomes

$$\begin{aligned} \frac{d}{dt}\left(\rho^{(2)}_{g4}\right)_{k,q}\Big|_{\text{LASER}} = & \left(\frac{1}{2}-\alpha\right)\frac{L_g}{9}\left[-(W_{g4,e4}W^{\dagger}_{e4,g4})_{k,q} + \frac{\xi_k(e4\to g4)}{\Gamma'_c}(W^{\dagger}_{e4,g4}W_{g4,e4})_{k,q}\right] \\ & + \left(\frac{1}{2}-\alpha\right)\frac{L_{eg}}{9}\left[-(W_{g4,e3}W^{\dagger}_{e3,g4})_{k,q} + \frac{\xi_k(e3\to g4)}{\Gamma'_c}(W^{\dagger}_{e3,g4}W_{g4,e3})_{k,q}\right] \\ & + \left(\frac{1}{2}+\alpha\right)\frac{1}{7}\left[L_0\frac{\xi_k(e4\to g4)}{\Gamma'_c}(W^{\dagger}_{e4,g3}W_{g3,e4})_{k,q} + L_e\frac{\xi_k(e3\to g4)}{\Gamma'_c}(W^{\dagger}_{e3,g3}W_{g3,e3})_{k,q}\right]. \end{aligned} \tag{A10}$$

Using standard methods (see [26]), the irreducible components of $W\,W^{\dagger}$ and $W^{\dagger}W$ can be worked out:

$$(W_{g_i,e_j}W^{\dagger}_{e_j,g_i})_{k,q} = E_0^2\langle F_{e_j}||\mathbf{d}||F_{g_i}\rangle^2(-1)^{F_{e_j}-F_{g_i}} \begin{Bmatrix} 1 & 1 & k \\ F_{g_i} & F_{g_i} & F_{e_j} \end{Bmatrix}(-1)^q\mathbb{E}_{k,-q}, \tag{A11a}$$

$$(W^{\dagger}_{e_j,g_i}W_{g_i,e_j})_{k,q} = E_0^2\langle F_{e_j}||\mathbf{d}||F_{g_i}\rangle^2(-1)^{F_{g_i}-F_{e_j}} \begin{Bmatrix} 1 & 1 & k \\ F_{e_j} & F_{e_j} & F_{g_i} \end{Bmatrix}(-1)^q\mathbb{E}_{k,-q}. \tag{A11b}$$

The reduced matrix element of the dipole can be rewritten as [32]

$$\begin{aligned} \langle F_{e_j}||\mathbf{d}||F_{g_i}\rangle &\equiv \langle (J_eI)F_{e_j}||\mathbf{d}||(J_gI)F_{g_i}\rangle \\ &= (-1)^{J_e+I+F_{g_i}+1}\sqrt{(2F_{e_j}+1)(2F_{g_i}+1)}\begin{Bmatrix} F_{e_j} & 1 & F_{g_i} \\ J_g & I & J_e \end{Bmatrix}\langle J_e||\mathbf{d}||J_g\rangle, \end{aligned} \tag{A12}$$

while the polarization tensor $\mathbb{E}_{k,q}$ is constructed from the laser polarization vector as

$$\mathbb{E}_{K,Q} = (-1)^{K+Q}\sqrt{2K+1}\sum_{q,q'=-1}^{1}\begin{pmatrix} 1 & 1 & K \\ q & q' & Q \end{pmatrix}(\epsilon^*)_{-q}\,\epsilon_{-q'}, \tag{A13}$$

which for circular σ^+ polarization becomes

$$\mathbb{E}_{k,q} = -\delta_{q,0}\left(\frac{1}{\sqrt{3}}\delta_{k,0} + \frac{1}{\sqrt{2}}\delta_{k,1} + \frac{1}{\sqrt{6}}\delta_{k,2}\right). \tag{A14}$$

Putting this all together, Eq. (A10) becomes

$$\begin{aligned} \frac{d}{dt}\left(\rho^{(2)}_{g4}\right)_{1,q}\Big|_{\text{LASER}} = & -\frac{\sqrt{15}}{20736}E_0^2\langle J_e||\mathbf{d}||J_g\rangle^2\frac{1}{1+r}[(1-2\alpha)(29+48r)\,L_g \\ & + 21(1-2\alpha)(25+16r)L_{eg} - 171(1+2\alpha)L_0 - 27(1+2\alpha)L_e]\delta_{q,0}, \end{aligned} \tag{A15}$$

where $r = \Gamma'_c/\,\Gamma$. Dropping the constant (irrelevant at this order of approximation) in front of the expression, this is exactly the $P(t)$ function used in Eq. (9). The time dependence arises from the laser modulation; that is, in Eq. (A3) the substitution $\delta \to \delta_0 + \Delta\sin\Omega t$.

The Fourier coefficients P_n of Eq. (9) have an analytical form. In fact redoing the steps of [33], one finds ($n \geqslant 0$)

$$\begin{aligned} P_n^{(0)} &\equiv \frac{\Omega}{2\pi}\int_0^{2\pi/\Omega} e^{-i\,n\,\Omega\,t}\,L_0(t)dt = \frac{1}{2\pi}\int_0^{2\pi} e^{-i\,n\,\theta}\,\frac{G}{G^2+(\delta_0+\Delta\sin\theta)^2}d\theta \\ &= \frac{1}{2}\int_{-\infty}^{+\infty} J_n(z\Delta)e^{i\,z\,\delta_0}e^{-G\,|z|}dz = \begin{cases} \text{Re}(I_n) & n \text{ even}, \\ i\,\text{Im}(I_n) & n \text{ odd}, \end{cases} \end{aligned} \tag{A16}$$

where

$$I_n \equiv \int_0^{+\infty} J_n(z\Delta)e^{i\,z\,\delta_0}e^{-G\,z}dz = \frac{1}{\Delta^n}\frac{[\sqrt{(G-i\delta_0)^2+\Delta^2}-(G-i\delta_0)]^n}{\sqrt{(G-i\delta_0)^2+\Delta^2}} \tag{A17}$$

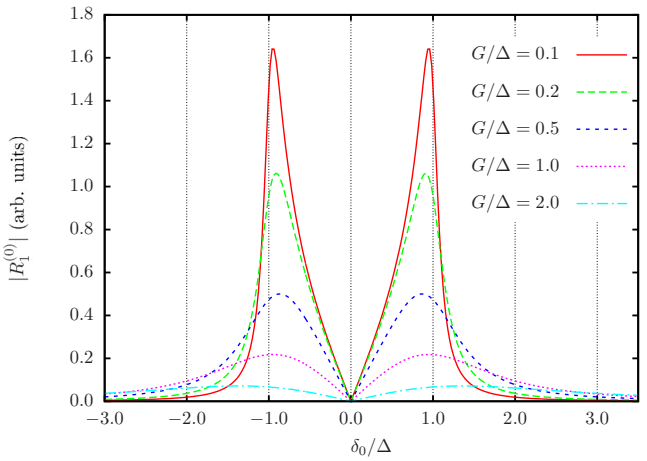

FIG. 6. Typical profile obtained from the excitation of a single transition. The peaks are located in correspondence with $\delta_0 \approx \pm\Delta$ for $G/\Delta \lesssim 1$. At larger values of G the peaks broaden and start shifting in opposite directions.

and the last step follows from formula (6.611) of [34]. So the first-harmonic coefficient reads [see also Eq. (13)]

$$R_1^{(0)} = -\frac{1}{\Delta}\mathrm{Im}\left(\frac{G - i\delta_0}{\Delta}\frac{1}{\sqrt{1+\left(\frac{G-i\delta_0}{\Delta}\right)^2}}\right), \tag{A18}$$

which can be rewritten using the dispersive and absorptive profiles

$$\mathcal{D}(\delta_0) = \frac{\delta_0 - \Delta}{(\delta_0-\Delta)^2 + G^2} - \frac{\delta_0 + \Delta}{(\delta_0+\Delta)^2 + G^2}, \tag{A19a}$$

$$\mathcal{L}(\delta_0) = \frac{1}{(\delta_0-\Delta)^2 + G^2} + \frac{1}{(\delta_0+\Delta)^2 + G^2} \tag{A19b}$$

as

$$R_1^{(0)} = -\frac{1}{\sqrt{2}\Delta}\,\mathrm{sgn}(-\delta_0)\left[\sqrt{1 + \Delta\frac{G^2 + 3\Delta^2/4}{G^2+\Delta^2}\left(\mathcal{D}(\delta_0) + \frac{\Delta^2}{4G^2+3\Delta^2}\mathcal{L}(\delta_0)\right)} - 1 - (\Delta/2)\mathcal{D}(\delta_0)\right]^{1/2}. \tag{A20}$$

This is the contribution of $L_0(t)$ that is the $F_g = 3 \to F_e = 4$ line, and it is shown in Fig. 6.

Similar expressions hold for the other transitions, and adding all of them together with the coefficients of Eq. (A15), we obtain the whole R_1, which contains the dependence from the laser modulation parameters.

[1] W. Happer, Y.-Y. Jau, and T. Walker, *Optically Pumped Atoms* (Wiley-VCH, Leipzig, 2010).
[2] W. Happer, Rev. Mod. Phys. **44**, 169 (1972).
[3] H. J. Metcalf and P. van der Straten, *Laser Cooling and Trapping* (Springer, New York, 1999).
[4] M. A. abd Ruvin Ferber, *Optical Polarization of Molecules* (Cambridge University Press, Cambridge, 2005).
[5] E. B. Aleksandrov and A. K. Vershovskii, Phys. Usp. **52**, 573 (2009).
[6] L. Lenci, A. Auyuanet, S. Barreiro, P. Valente, A. Lezama, and H. Failache, Phys. Rev. A **89**, 043836 (2014).
[7] D. Budker and M. Romalis, Nat. Phys. **3**, 227 (2007).
[8] D. Suter and J. Mlynek, Phys. Rev. A **43**, 6124 (1991).
[9] V. Schultze, R. Ijsselsteijn, T. Scholtes, S. Woetzel, and H.-G. Meyer, Opt. Express **20**, 14201 (2012).
[10] M. Rosatzin, D. Suter, W. Lange, and J. Mlynek, J. Opt. Soc. Am. B **7**, 1231 (1990).
[11] H. Klepel and D. Suter, Opt. Commun. **90**, 46 (1992).
[12] E. Breschi, Z. D. Gruijc, P. Knowles, and A. Weis, Phys. Rev. A **88**, 022506 (2013).
[13] E. Breschi, Z. D. Grujic, P. Knowles, and A. Weis, Appl. Phys. Lett. **104**, 023501 (2014).
[14] G. Bevilacqua and E. Breschi, Phys. Rev. A **89**, 062507 (2014).
[15] J. Belfi, G. Bevilacqua, V. Biancalana, Y. Dancheva, and L. Moi, J. Opt. Soc. Am. B **24**, 1482 (2007).
[16] V. Acosta, M. P. Ledbetter, S. M. Rochester, D. Budker, D. F. J. Kimball, D. C. Hovde, W. Gawlik, S. Pustelny, J. Zachorowski, and V. V. Yashchuk, Phys. Rev. A **73**, 053404 (2006).
[17] T. Zigdon, A. D. Wilson-Gordon, S. Guttikonda, E. J. Bahr, O. Neitzke, S. M. Rochester, and D. Budker, Opt. Express **18**, 25494 (2010).
[18] G. Bevilacqua, V. Biancalana, Y. Dancheva, and L. Moi, Phys. Rev. A **85**, 042510 (2012).
[19] D. Sheng, S. Li, N. Dural, and M. V. Romalis, Phys. Rev. Lett. **110**, 160802 (2013).
[20] T. Wolf, P. Neumann, K. Nakamura, H. Sumiya, T. Ohshima, J. Isoya, and J. Wrachtrup, Phys. Rev. X **5**, 041001 (2015).
[21] I. Sydoryk, N. N. Bezuglov, I. I. Beterov, K. Miculis, E. Saks, A. Janovs, P. Spels, and A. Ekers, Phys. Rev. A **77**, 042511 (2008).
[22] G. Bevilacqua, V. Biancalana, P. Chessa, and Y. Dancheva, Appl. Phys. B **122**, 1 (2016).
[23] G. Bevilacqua, V. Biancalana, Y. Dancheva, and L. Moi, Ann. Rep. NMR Spectrosc. **78**, 103 (2013).
[24] G. Bevilacqua, V. Biancalana, Y. Dancheva, and L. Moi, J. Magn. Reson. **201**, 222 (2009).
[25] G. Bevilacqua, V. Biancalana, A. B.-A. Baranga, Y. Dancheva, and C. Rossi, J. Magn. Reson. **263**, 65 (2016).
[26] A. Omont, *Irreducible Components of the Density Matrix: Application to Optical Pumping*, Progress in Quantum Electronics (Pergamon, Oxford, 1977).
[27] J. J. Sakurai and J. J. Napolitano, *Modern Quantum Mechanics*, 2nd ed. (Addison Wesley, Boston, 2010).
[28] F. A. Franz and J. R. Franz, Phys. Rev. **148**, 82 (1966).
[29] W. E. Baylis, *Progress in Atomic Spectroscopy: Part B* (Springer, Boston, 1979), pp. 1227–1297.

[30] S. Stenholm, *Foundations of Laser Spectroscopy*, Dover Books on Physics (Dover, Mineola, NY, 2005).
[31] M. Dumont and B. Decomps, J. Phys. (Paris) **29**, 181 (1968).
[32] B. R. Judd, *Operator Techniques in Atomic Spectroscopy* (Princeton University Press, Princeton, NJ, 2014).
[33] R. Arndt, J. Appl. Phys. **36**, 2522 (1965).
[34] I. S. Gradshteyn and I. M. Ryzhik, *Table of Integrals, Series, and Products*, 7th ed., translated from Russian, edited by A. Jeffrey and D. Zwillinger (Academic, Amsterdam, 2007).